The Effect of Asian Dust Aerosols on Cloud Properties and Radiative Forcing from MODIS and CERES

Jianping Huang[1,3], Patrick Minnis[2], Bing Lin[2], Tianhe Wang[1], Yuhong Yi[3]
Yongxiang Hu[2], Sunny Sun-Mack[4], and Kirk Ayers[3]

[1]College of Atmospheric Sciences, Lanzhou University, Lanzhou, 73000
[2]NASA Langley Research Center, Hampton, VA, 23681
[3]AS & M, One Enterprise Parkway, Hampton, VA, 23666
[4]SAIC, One Enterprise Parkway, Hampton, VA, 23666

Submitted to Geophysical Research Letters

September 2005

Abstract

The effects of dust storms on cloud properties and radiative forcing are analyzed over northwestern China from April 2001 to June 2004 using data collected by the Moderate Resolution Imaging Spectroradiometer (MODIS) and Clouds and the Earth's Radiant Energy System (CERES) instruments on the *Aqua* and *Terra* satellites. On average, ice cloud effective particle diameter, optical depth and ice water path of the cirrus clouds under dust polluted conditions are 11%, 32.8%, and 42% less, respectively, than those derived from ice clouds in dust-free atmospheric environments. The humidity differences are larger in the dusty region than in the dust-free region, and may be caused by removal of moisture by wet dust precipitation. Due to changes in cloud microphysics, the instantaneous net radiative forcing is reduced from -71.2 W/m^2 for dust contaminated clouds to -182.7 W/m^2 for dust-free clouds. The reduced cooling effects of dusts may lead to a net warming of 1 W/m^2, which, if confirmed, would be the strongest aerosol forcing during later winter and early spring dust storm seasons over the studied region.

INDEX TERMS: 0305 Atmospheric Composition and Structure: Aerosols and particles (0345, 4801); 0320 Atmospheric Composition and Structure: Cloud physics and chemistry; 3359 Meteorology and Atmospheric Dynamics: Radiative process; 1620 Global Change: Climate dynamics (3309).

1. Introduction

Dust storms that blanket northeast Asia have serious impacts on the global climate system. These storms originate in the Taklamakan Desert of China and the Gobi Desert of China and Mongolia and occur most frequently in late winter and early spring. The dust aerosols of these storms are capable of traveling thousands of kilometers at high altitude and flow out from the continent to the open sea near Korea and Japan [*Haywood et al.*, 1999; *Higurashi and Nakajima*, 2002; *Takemura et al.*, 2002]. These aerosols not only reflect the incoming solar radiation to space, but also modify cloud properties by changing the number concentration of cloud droplets, which alters both cloud optical depth and cloud lifetime [*Twomey et al.*, 1984; *Ackerman et al.*, 2000; *Liu et al.*, 2003]. In addition, the aerosols can affect the radiative heating structure of the atmosphere, thereby changing the clouds and atmospheric general circulation.

Recently, special attention has been dedicated to cloud interactions with desert aerosol particles [*Bréon et al.*, 2002; *DeMott et al.*, 2003; *Kawamoto and Nakajima*, 2003]. Using satellite and aircraft observations, *Rosenfeld et al.* [2001] found that clouds forming within desert dust contain small droplets and produce little precipitation by drop coalescence. The dramatic correlation of the presence of Asian dust and ice formation in modestly super-cooled altocumulus clouds was previously demonstrated by *Sassen* [2002]. *Levi and Rosenfeld* [1996] observed similar increase in ice nuclei concentrations during dust storm periods in Israel. The action of Saharan dust particles as ice nuclei was even used to explain the impacts of cloud seeding experiments in Israel [*Rosenfeld and Nirel*, 1996].

Despite the fact that the Taklamakan and Gobi Deserts are major sources of dust aerosols, there have been few studies focusing on the effect of Asian dust aerosols on clouds, especially ice cloud properties and radiative forcings. This study investigates the influence of Asian dusts on ice cloud properties using the MODerate resolution Imaging Spectroradiometer (MODIS) and Clouds and the Earth's Radiant Energy System (CERES) scanner data. The effect of dust aerosols on clouds is evaluated by comparing the properties and radiative forcings of dust-free and dusty clouds. This assessment should lead to a better understanding of the interactions among dust aerosols, clouds and radiation fields.

2. Data and Methodology

The Visible-Infrared-Solar-infrared-Split-window Technique (VISST) was used to derive daytime cloud properties from *Aqua* and *Terra* MODIS data taken between April 2001 and June 2004. The retrieved cloud properties include cloud effective droplet radius (r_e) or ice crystal diameter (De), optical depth (τ), effective cloud top temperature (Te), and water path (WP). VISST is a 4-channel update of the retrieval algorithm of *Minnis et al.* [1995]. It utilizes parameterizations of radiative transfer calculations for 7 water droplet and 9 ice crystal size distributions [*Minnis et al.*, 1998] to compute theoretical radiances that are matched with satellite-observed visible and near-infrared (0.65 and 3.9 μm) reflectances and 3.9, 10.8, and 12.0 μm brightness temperatures. The method accounts for the contributions of the surface and atmosphere to the radiance in each channel. Flux measurements from CERES are used to estimate the instantaneous radiative forcings. The CERES instruments measure broadband radiances at the TOA in

three spectral regions (0.2 - 5.0 μm; 8 - 14 μm; 5 - 100 μm) at a spatial resolution of about 20 km at nadir [*Wielicki et al.*, 1996]. The CERES Meteorological, Ozone, and Aerosol (MOA) data, including vertical profiles of temperature and humidity from the Goddard Earth Observing System Assimilation System [*Bloom et al.,* 2005], are used to analyze meteorological conditions.

3. Analysis and Results

Figure 1a shows images from MODIS data for a dust storm case on 27 March 2004 over northwestern China. The existence of dust enhances the reflectance as seen in the true-color composite image (Figure 1a). *Ackerman* [1997] showed that the brightness temperature (BT) difference between the 11 and 12 μm channels (T45) is negative for dust because dust layers have a higher emissivity at 12 μm than at 11 μm. In this case, the clouds are distinct from the dust in the T45 image (Figure 1b). The average T45 is less than –2.0 K for a pure dust region and larger than 0 K in the cloudy regions. In dusty areas with clouds, the T45 signals from dust and clouds tend to cancel each other and are not very useful for cloud identification.

To detect cloud modifications induced by dust aerosols, four regions are selected to represent the dusts and clouds in different environments. Box 1 (hereafter DUST) in Figure 1b represents the cloud-free dust region. Box 2 (hereafter, CLD) denotes an area where clouds occurred in a dust-free atmosphere. Box 3 (hereafter, PCOD) includes partial clouds in a dusty region. Box 4 (hereafter, COD) represents overcast clouds in dusty conditions. The CLD and COD regions are selected based on surface meteorology

station observations. Table 1 shows the information for the ten carefully selected dust storm cases used in this study.

Histograms of the pixel-level ice cloud properties for each category from the 10 cases in Table 1 are shown in Figure 2. The effect of dust on cloud properties is evident in the D_e (Fig. 2a), τ (Fig. 2b), and WP (Fig. 2c) frequency distributions. The average D_e drops from 54.0 μm in the CLD regions to 48.0 μm in the COD areas. Smaller values of D_e occur more frequently for both the PCOD and COD regions compared to the CLD regions. The mean τ over CLD regions (Figure 2b) is 21.9, which is 12.8 and 7.2 greater than the averaged τ of the PCOD and COD regions, respectively. Consequently, the mean WP values for PCOD and COD regions (Figure 2c) are also considerably smaller than those from CLD regions. The mean WP decreases from 396.2 g/m^2 to 128.7 and 230.7 g/m^2 for the PCOD and COD regions, respectively. The T_e values (Fig. 2d) for the CLD and COD regions, however, are very close, which suggests that the cloud top heights are nearly identical for these regions. The mean T_e (241.3 K) in PCOD regions (Fig. 2d) is higher than in the other two regions, possibly due to the effect of dust on middle-low level atmospheric conditions (see discussions below).

The regional mean aerosol top temperature, retrieved from the infrared (11 μm) channel, is about 224.6 K in the DUST region, which is lower than the cloud top temperature in the CLD, COD or PCOD regions. Although they may not be the best representation of the temperature of the dust aerosol layer top, the infrared measurements suggest that dust aerosol layers associated with dust storms cover most cloud altitudes and, therefore, are probably mixing with the clouds.

Figure 3 shows the cloud properties in the CLD and COD regions as a function of T_e. The cloud properties in COD regions represent the combined effects of upper-layer clouds and lower-layer dust aerosols. For dusty cloud tops with temperatures in the range of 230 K< Te ≤ 245 K, the D_e means (Fig. 3a) are less than those for dust-free clouds by more than 18%. The ice crystal size of the dusty clouds is generally smaller suggesting that in COD cases, the dust aerosols are serving as ice nuclei and induce more small ice particles. The effects of dust aerosols are even more significant on τ (Figure 3b) and WP (Figure 3c). For the very cold dusty clouds (Te ≤ 245 K), mean τ and WP are less than those from dust-free clouds by more than 40% and 27%, respectively, due to reduced humidity and less condensation caused by mixing of dry dust air masses with humid cloud air masses in lower atmospheric layers. Regionally averaged MOA vertical profiles of relative humidity (Table 2) show that the relative humidity is about 10% less in the COD region than in the CLD region for the middle and low atmosphere (500 - 1000 hPa). However, in upper layers (200 – 500 hPa), the relative humidity is similar in the dusty (COD and PCOD) and dust-free regions (CLD), which suggests that the potential for generating high ice cloud hydrometeors may be the same in upper layers. The humidity differences in upper and lower layers between dusty and dust-free regions may be caused by removal of moisture by wet dust precipitation since the mixing speed is much faster in lower layers than in upper layers.

The top-of-atmosphere (TOA) radiative forcing is defined as:

$$\begin{aligned} C_{sw} &= F_{clr}^{sw} - F^{sw} \\ C_{lw} &= F_{clr}^{lw} - F^{lw} \\ C_{net} &= C_{sw} + C_{lw} \end{aligned} \qquad (1)$$

where F_{clr}^{sw} and F_{clr}^{lw} are the CERES clear sky broadband shortwave (SW) and longwave (LW) fluxes at the TOA, respectively. F^{sw} and F^{lw} are the SW and LW fluxes at the TOA in the presence of dust aerosol, cloud, or both. The regional, averaged radiative forcing derived for the four regions defined in Figure 1b are listed in Table 3. For clouds growing in the presence of dust, the instantaneous TOA SW radiative forcing values are about -144.9 W/m^2 for PCOD region and -150.3 W/m^2 for COD region. The clouds developing in CLD regions yield the most negative SW forcing (-296 W/m^2), which is about 50% stronger than those in PCOD and COD regions. For LW radiative forcing, the dust-free cloud (CLD) is around 113.3 W/m^2, which is 43% and 30% greater than the LW forcing from PCOD and COD regions, respectively. The instantaneous TOA net radiative forcing for the CLD region is about -182.7 W/m^2, which is more than 2 and 4 times as large as the values from the dusty cloudy (PCOD and COD) and the DUST regions, respectively. If the diurnal cycle of the atmosphere is considered, the estimated mean net radiative forcing is -35, -8, 4 and 3 W/m^2 for CLD, PCOD, COD and DUST regions, respectively. Thus, the existence of dusts under clouds significantly reduces the cooling effect of clouds. These reduced cooling effects of dusts for PCOD (27W/m^2) and COD (39 W/m^2) regions on clouds can be considered as actual warming effects of dust aerosols. Since the long-term averaged dust storm frequency of occurrence based on surface meteorology station observations is about 3.7%, assuming the frequencies of occurrences of PCOD, COD and DUST in dusty cases are the same, the averaged climate forcing (warming) of dust storms is about 1 W/m^2.

4. Conclusions and Discussions

This study shows the effect of Asian dust aerosols on ice cloud properties and TOA radiative forcings. Analysis of the satellite observations indicates that the D_e values of dusty clouds are considerably smaller than those from dust-free clouds. It suggests that dust aerosols may act as cloud condensation nuclei and cause changes in the size of ice cloud particles. *DeMott et al.* [2003] provided evidence for the strong ice nucleating function of Saharan dust aerosols as measured at long distances from the source. The current results also show that the τ and WP of dusty clouds are much less than those from dust-free clouds. Previous studies [*Twomey*, 1984; *Albrecht*, 1989] indicated constant or increased cloud liquid WP associated with high aerosol concentrations for water clouds over oceans. Current results suggest a different effect of dust aerosols on relatively dry upper-level air masses, high clouds, and ice cloud condensation over arid or semi-arid regions. The key issue may be related to the mixing of different air masses. The most common dust storms in East Asia are those caused by strong winds behind a cold front. The colder dry air masses associated with the cold fronts are quickly mixed with relatively warm and humid air masses in the lower layers of the atmosphere, which reduces a significant portion of the water vapor through wet deposition or light rainfall. In this case, the impact of dust aerosols on radiative forcing becomes very complex. For DUST regions, the dust aerosol has a cooling effect at the TOA in daytimes and net warming when both day and night times are considered. These aerosols also cancel or reduce the cloud cooling effect at the TOA in PCOD and COD regions due to decreasing water path. If confirmed, the net radiative forcing (1 W/m^2) of dust storms estimated from the current study will be the strongest aerosol forcing in the studied region during

dust storm seasons, and have profound warming influences on the atmospheric general circulation and climate.

The results presented here represent only a first step in better understanding of the effect of Asian dust on climate. The cloud properties estimated in this study are basically from daytimes and were taken from limited events. The aerosol-related changes in the cloud properties reported here may not be the same as nighttime changes. More observations of the dust storm properties for full diurnal cycle need to be examined to develop robust statistics in the future studies.

Acknowledgment

This research is supported by NASA Science Mission through the CERES Project. The CERES data were obtained from the NASA Earth Observing System Data and Information System, Distributed Active Archive Center (DAAC) at the Langley Research Center.

References

Ackerman, S. A., 1997, Remote sensing aerosols using satellite infrared observations, *J. Geophys. Res., 102*(D14) 17,069– 17,080.

Ackerman, S. A., O. B. Toon, D. E. Stevens, A. J. Heymsfield, V. Ramanathan, and E. J. Welton (2000), Reduction of tropical cloudiness by soot, *Science, 288*, 1042 – 1047.

Albrecht, B.A. (1989), Aerosols, cloud microphysics, and fractional cloudiness, *Science, 245*, 1227-1230.

Bloom, S., A. da Silva, D. Dee, M. Bosilovich, J.-D. Chern, S. Pawson, S. Schubert, M. Sienkiewicz, I. Stajner, W.-W. Tan, M.-L. Wu (2005), Documentation and Validation of the Goddard Earth Observing System (GEOS) Data Assimilation System - Version 4, *Technical Report Series on Global Modeling and Data Assimilation 104606*, 26.

Bréon, F.-M., D. Tanré, and S. Generoso (2002), Aerosol effect on cloud droplet size monitored from satellite, *Science*, *295*, 834-838.

DeMott, P. J., K. Sassen, M. Poellot, D. Baumgardner, D. C. Rogers, S. Brooks, A. J. Prenni, and S. M. Kreidenweis (2003), African dust aerosols as atmospheric ice nuclei, *Geophys. Res. Lett*., *30,* 1732, doi:10.1029/2003GL017410.

Haywood, J. M., V. Ramaswamy, and B. J. Soden (1999), Tropospheric aerosol climate forcing in clear-sky satellite observations over the oceans, *Science*, *283*, 1299–1305.

Higurashi, A., and T. Nakajima (2002), Detection of aerosol types over the East China Sea near Japan from four-channel satellite data, *Geophys. Res. Lett., 29*, 1836, doi:10.1029/2002GL015357.

Levi, Y., and D. Rosenfeld (1996)**,** Ice nuclei, rainwater chemical composition, and static cloud seeding effects in Israel, *J. Appl. Meteorol.*, *35*, 1494–1501.

Liu, G., H. Shao, J. A. Coakley, J. A. Curry, J. A. Haggerty, and M. A. Tschudi (2003), Retrieval of cloud droplet size from visible and microwave radiometric measurements during INDOEX: Implication to aerosols' indirect radiative effect, *J. Geophys. Res., 108(D1)*, 4006, doi:10.1029/2001JD001395.

Kawamoto, K., and T. Nakajima (2003), Seasonal variation of cloud particle size from AVHRR remote sensing, *Geophys. Res. Lett*., *30*, 1810-1813.

Minnis, P., D. P. Garber, D. F. Young, R. F. Arduini, and Y. Takano (1998), Parameterization of reflectance and effective emittance for satellite remote sensing of cloud properties, *J. Atmos. Sci.*, 55, 3313-3339.

Minnis, P., D. P. Kratz, J. A. Coakley, Jr., M. D. King, D. Garber, P. Heck, S. Mayor, D. F. Young, and R. Arduini. (1995), Cloud Optical Property Retrieval (Subsystem 4.3). "Clouds and the Earth's Radiant Energy System (CERES) Algorithm Theoretical Basis Document, Volume III: Cloud Analyses and Radiance Inversions (Subsystem 4)", *NASA RP 1376 Vol. 3*, edited by CERES Science Team, pp. 135-176.

Rosenfeld, D., and R. Nirel (1996)**,** Seeding effectiveness - The interaction of desert dust and the southern margins of rain cloud systems in Israel, *J. Appl. Meteorol.*, *35*, 1502–1510.

Rosenfeld, D., Y. Rudich, and R. Lahav (2001)**,** Desert dust suppressing precipitation: a possible desertification feedback loop, *Proceedings of the National Academy of Sciences*, *98*(11), 5975–5980.

Sassen, K. (2002), Indirect climate forcing over the western US from Asian dust storms, *Geophys. Res. Lett.*, *29,* 1029, doi:10.1029/2001GL014034.

Takemura, T., I. Uno, T. Nakajima, A. Higurashi, and I. Sano (2002), Modeling study of long-range transport of Asian dust and anthropogenic aerosols from East Asia, *Geophys. Res. Lett.*, *29*, 2158, doi:10.1029/2002GL016251.

Twomey, S., M. Piepgrass, and T. L. Wolfe (1984), An assessment of the impact of pollution on global cloud albedo, *Tellus, 36B*, 356-366.

Wielicki, B. A., B. R. Barkstrom, E. F. Harrison, R. B. Lee III, G. L. Smith, and J. E. Cooper (1996), Clouds and the Earth's Radiant Energy System (CERES): an earth observing system experiment, *Bull. Amer. Meteor. Soc.*, *77*, 853–868.

Table 1. Ten dust cases images used in this study

Image	Date	GMT	Lat（°N）	Lon（°E）	SAT
1	2004/03/27	05:15	40.0-50.0	104.0-118.0	Aqua
2	2003/04/17	07:00	35.0-45.0	73.0-87.0	Aqua
3	2003/04/17	05:25	35.0-45.0	73.0-87.0	Terra
4	2003/04/09	06:15	35.0-45.0	72.0-86.0	Aqua
5	2003/04/09	07:50	35.0-45.0	72.0-86.0	Terra
6	2003/03/26	04:20	38.0-48.0	118.0-132.0	Aqua
7	2004/03/09	05:30	40.0-50.0	102.0-116.0	Aqua
8	2004/05/08	04:15	40.0-50.0	118.0-132.0	Aqua
9	2003/05/11	04:35	34.0-44.0	75.0-89.0	Terra
10	2001/04/07	04:20	33.0-43.0	100.0-114.0	Terra

Table 2. Comparison of the averaged humidity between different regions

	Dust	CLD	PCOD	COD
200-500 hPa	43.5%	58.5%	59.9%	66.9%
500-1000 hPa	36.3%	57.5%	46.1%	47.6%

Table 3. Comparison of the averaged radiative forcing (W/m^2) at the TOA

	Dust	CLD	PCOD	COD
SW	-89.9	-296.0	-144.9	-150.3
LW	47.9	113.3	64.0	79.1
Net	-42.0	-182.7	-80.9	-71.2

Figure Captions

Figure 1. a) The true color composite (upper panel) over Northwest China, in which channel 0.65μm, 0.56μm and 0.47μm are associated with red, green and blue colors, respectively; b) The brightness temperature (BT) difference (lower panel) between 11 and 12 μm channels (T45). The square box 1 is the pure dust region (DUST), box 2 the cloud in dust-free cloud region (CLD), box 3 the partial clouds over dust region (PCOD), and box 4 the clouds over dust region (COD).

Figure 2. Comparison of the ice cloud properties over the dust-free region (open bar), partial clouds over the dust region (gray bar), and overcast clouds over the dust region (black bar) for (a) ice diameter, (b) optical depth, (c) ice water path and (d) effective cloud top temperature. The histogram intervals are 10μm for (a), 10 for (b), 200 g/m^2 for (c), and 5 K for (d).

Figure 3. Comparison of the averaged (ten cases) ice cloud properties for CLD with COD region as a function of effective cloud top temperature T_e for (a) ice particle effective diameter (D_e), (b) optical depth (OPD), and (c) ice water path (IWP).

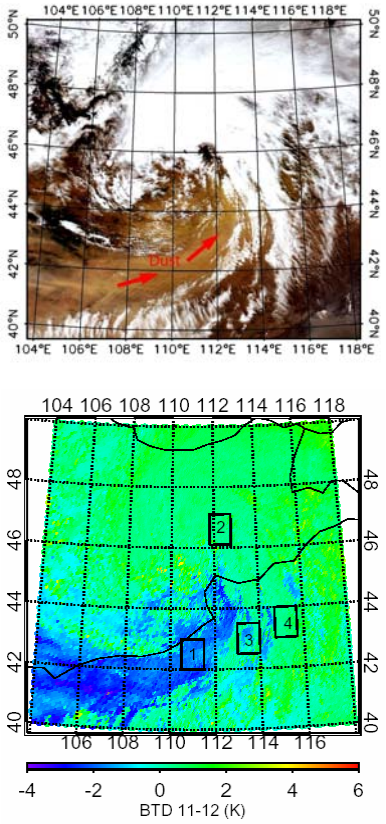

Figure 1. a) The true color composite (upper panel) over Northwestern China, in which channel 0.65μm, 0.56μm and 0.47μm are associated with red, green and blue colors, respectively; b) The brightness temperature (BT) difference (lower panel) between 11 and 12 μm channels (T45). The square box 1 is the pure dust region (DUST), box 2 the cloud in dust-free cloud region (CLD), box 3 the partial clouds over dust region (PCOD), and box 4 the clouds over dust region (COD).

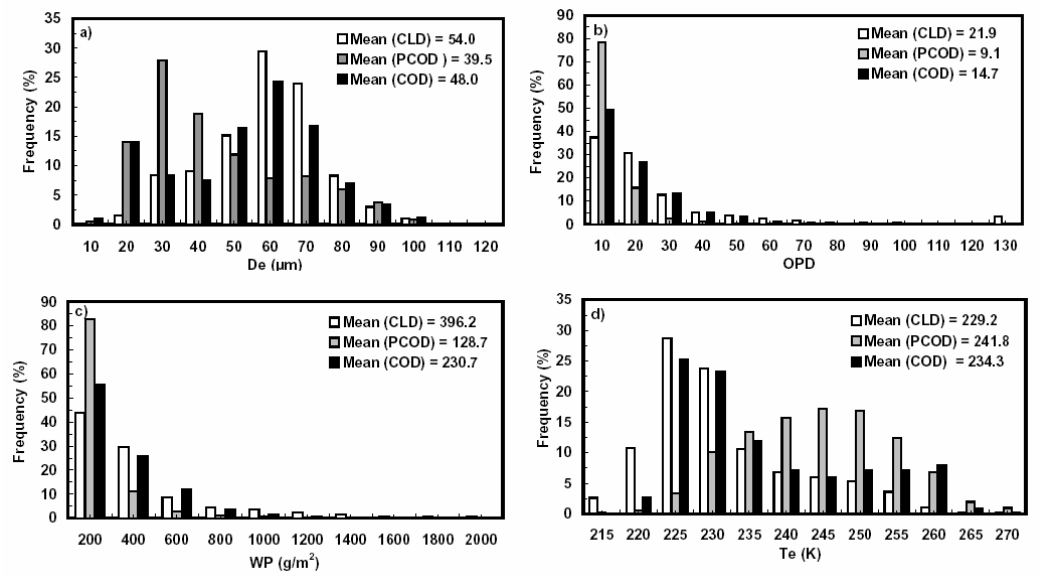

Figure 2. Comparison of the ice cloud properties over the dust-free region (open bar), partial clouds over the dust region (gray bar), and overcast clouds over the dust region (black bar) for (a) ice diameter, (b) optical depth, (c) ice water path and (d) effective cloud top temperature. The histogram intervals are 10μm for (a), 10 for (b), 200 g/m^2 for (c), and 5 K for (d).

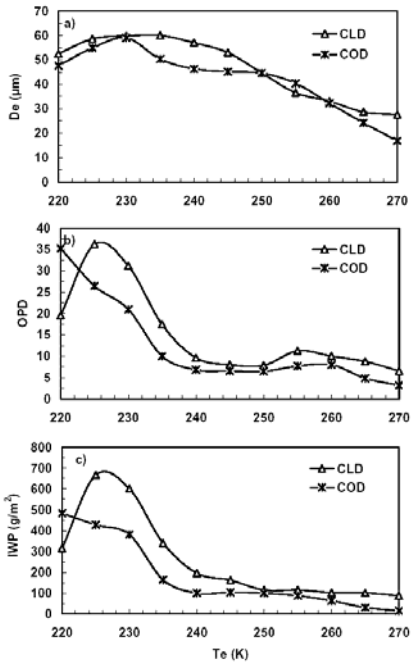

Figure 3. Comparison of the averaged (ten cases) ice cloud properties for CLD with COD region as a function of effective cloud top temperature T_e for (a) ice particle effective diameter (D_e), (b) optical depth (OPD), and (c) ice water path (IWP).